An ultracompact X-ray source based on a laser-plasma undulator

I.A. Andriyash, R. Lehe, Agustin Lifschitz, Cédric Thaury, Jean-Marcel Rax, K. Krushelnick, Victor Malka

An ultra-compact X-ray source based on a laser-plasma undulator

I.A. Andriyash,[1,*] R. Lehe,[1] A. Lifschitz,[1] C. Thaury,[1] J.-M. Rax,[1,2] K. Krushelnik,[3] and V. Malka[1,†]

[1] *Laboratoire d'Optique Appliquée, ENSTA-ParisTech, CNRS, Ecole Polytechnique, UMR 7639, 91761 Palaiseau, France*

[2] *Universite-Paris XI, Orsay Cedex 91405, France*

[3] *Center for Ultrafast Optical Science, University of Michigan, Ann Arbor, Michigan 48109, USA*

The capability of plasmas to sustain ultra-high electric fields has attracted considerable interest over the last decades and gave rise to laser-plasma engineering. Today plasmas are commonly used for accelerating and collimating relativistic electrons, or to manipulate intense laser pulses. Here we propose an ultra-compact plasma undulator which combines plasma technology and nano-engineering. When coupled with a laser-plasma accelerator, this undulator constitutes a millimeter-size synchrotron radiation source of X-rays. The undulator consists of an array of nano-wires, which are ionized by the laser pulse exiting from the accelerator. The strong charge-separation field, arising around the wires, efficiently wiggles the laser-accelerated electrons. We demonstrate that this system can produce bright, collimated, and tunable beams of photons with 10-100 keV energies. This concept opens a path towards a new generation of compact synchrotron sources based on nano-structured plasmas.

Introduction

Today's brightest X-ray beams are generated by synchrotron radiation (SR) sources [1–3]. In industry, biology and basic research this radiation is used for ultrafast transient imaging with ångström resolution. Synchrotron radiation is produced by electrons, which are accelerated to relativistic energies and injected into a spatially modulated field. The electrons oscillate in this field and radiate light at a frequency which is the frequency of their own oscillations up-shifted by a factor $2\gamma_\mathrm{e}^2$, where $\gamma_\mathrm{e} = \varepsilon_\mathrm{e}/m_\mathrm{e}c^2$ is the Lorentz factor of an electron with an energy ε_e. In conventional SR sources, the undulating field is produced by a periodic structure of permanent magnets. For efficient X-rays generation, meter-long magnetic undulators with a period of $1-10$ centimeters are required. The relativistic electron beams are typically provided by large-scale accelerator facilities.

Laser-plasma technologies may offer a number of solutions for the development of next generation of light sources. Besides being the accelerating media in electron accelerators [4–8], laser plasmas can be used for instance as plasma mirrors [9] or non-linear media [10] to manipulate high-intensity laser pulses, or to collimate relativistic electrons [11]. Laser-plasma accelerators (LPA) have the potential to reduce the size of electron accelerators down to a few millimeters. Indeed, as an ionized medium, plasma can withstand much higher fields than the cavity walls in conventional accelerators, which are subject to electrical break-down. In LPA, an ultrashort laser pulse is focused in a gas media. The laser ionizes the gas and drives a copropagating plasma wave, in which electrons can be trapped and accelerated. State-of-the-art LPA deliver reproducible and quasi-monoenergetic electron beams with energies of hundreds of MeVs [8], and record values that exceed 3 GeV [12]. The electron beams have micrometer source sizes and carry electron currents of tens of kilo-Amperes. This extremely high electron flux suggests that LPA can produce very bright synchrotron radiation, that opens the path for a compact free electron laser [13].

Synchrotron radiation sources based on a combination of LPA and magnetic undulator have recently been demonstrated for visible light [14] and soft X-rays [15] emission. These experiments were performed with meter-scale magnetic undulators that were placed tens of centimeters after the exit of the accelerator. However, as the divergence of the electron beam in LPA is typically of a few milliradians, the electron flux can be reduced by four order of magnitude after a propagation of 10 cm. This rapid decrease of the electron flux strongly limits the brightness of SR sources based on LPA and a magnetic undulator, and has hindered the development of such sources.

In this letter, we present a synchrotron radiation source, which combines laser-plasma engineering and nano-structured target. The key new element of the proposed scheme is the use of a laser-plasma undulator instead of a magnetic undulator. The undulator consists of an array of cylindrical nano-wires arranged in a checkerboard pattern and oriented perpendicularly to the laser propagation. When ionized and heated by the laser field, the wires generate a strong electric field that bends the trajectories of the incoming relativistic electrons. Importantly, this undulator can be as small as a few micrometers. This makes the overall interaction length remarkably short and allows to take advantage of the high electron flux of LPA before it is reduced by the natural divergence of the beam.

*Electronic address: igor.andriyash@ensta-paristech.fr

†Electronic address: victor.malka@ensta-paristech.fr

Results

A. Parameters of laser-plasma undulator

The overall scheme of the proposed light source is presented in Fig. 1. We consider a 30-femtosecond pulse from a TW-class laser is focused into an ultrasonic gas jet. The laser ionizes the gas and drives a plasma wave in its wake. Some of the electrons of the gas are trapped in this wave and are accelerated up to a few hundreds of MeV. At the exit of the accelerator, the laser pulse and the electron beam propagate through a millimeter-scale vacuum space before entering the undulator region. The wires have a typical diameter of few hundreds of nanometers, and are 10-20 μm long.

The wires spacing along the electron propagation defines the undulator period λ_u. The transverse wires spacing determines the amplitude of the wiggling field, and thus the ability of the undulator to deviate the propagating electrons. In synchrotron radiation science, this ability is characterized by the undulator strength parameter K. This parameter can be defined as the amplitude of the oscillations of the particles normalized transverse momentum. The strength of an ideal magnetic undulator depends only on the amplitude of the undulator field B_0 and on its period, and is given by the relation $K = eB_0\lambda_\mathrm{u}/(2\pi m_\mathrm{e}c^2)$. In the nano-wire undulator, the wiggling field is strongly inhomogeneous, and each particle oscillate with different amplitude. In this case, one should consider the oscillations of individual particles to define the averaged K. In terms of produced radiation, the strength parameter separates the undulator $K \lesssim 1$ and wiggler $K \gg 1$ emission regimes [16]. In the undulator regime, electrons emit photons in a narrow energy band around the fundamental wavelength $\lambda_\mathrm{r} = \lambda_\mathrm{u}/(2\gamma_\mathrm{e}^2)$, while in the wiggler regime, they emit a broadband spectrum.

B. Interaction features

The analysis of the operation of a laser-plasma undulator can be divided in three parts: (i) the interaction of the laser field with an individual wire, (ii) the propagation of the laser pulse through the array of wires and (iii) the motion of the electrons in the undulator field and the related emission.

(i) The interaction of a high-power laser pulse with a solid wire leads to the creation of a plasma with a high electron density, on the surface of the wire. Such an over-critical plasma is opaque to the laser and thus the laser radiation only penetrates in a nanometer-thin sheath [17]. The electrons in this sheath are heated by the laser field in a process that strongly depends on the laser polarization. In particular, for a laser wave polarized perpendicularly to the wire, the electric field has a component normal to the wire surface, which enhances the heating, in a similar way to Brunel absorption [18]. Once the laser pulse has passed the wire, the expansion of the hot electrons produces a strong charge separation field on the wire surface. The field amplitude E_0 is estimated to be of the same order of magnitude as the laser amplitude E_las and it can be as high as a few teravolts per meter. The propagation of the laser and electron beams and generation of space charge field is shown in Fig. 2. Over the femtosecond interaction time, the laser which has an intensity $\sim 10^{19}$ W cm^{-2}, does not affect the ion core of the wires. The electrostatic field of the ionized wires remains quasi-constant on the time scale of the Coulomb explosion of the ions. For solid density plasmas this time is typically around a picosecond. For longer times, the wires will be destroyed by Coulomb explosion.

(ii) The energy lost by the laser in the interaction with each wire is either absorbed by hot electrons or carried away by the diffracted electromagnetic wave. A detailed analysis indicates that for the typical parameters presented in Table 1, diffraction losses dominate over the absorption. More precisely, the cylindrical electromagnetic wave that is reflected by the plasma wire carries a fraction $\eta_\mathrm{diff} \simeq \sqrt{2\pi}R_\mathrm{wire}/\sigma_\mathrm{las}$ of the total laser power. As the laser propagates through the array of wires, the diffraction losses lead to an exponential depletion of the laser intensity with the propagation distance $I_\mathrm{las}(x) \propto \exp(-x/l_\mathrm{loss})$. The characteristic length of energy deposition is given by $l_\mathrm{loss} = \lambda_\mathrm{u}\sigma_\mathrm{las}/(f\sqrt{2\pi}R_\mathrm{wire})$, where $f = \sum_j \exp(-y_j^2/2\sigma_\mathrm{las}^2)$ is the effective number of ionized wires, which takes into account the lesser value of the laser intensity at the transverse positions of the wires y_j. For parameters given in Table 1, the laser depletion length is estimated as $l_\mathrm{loss} = 0.2$ mm.

(iii) The wiggling motion of the electrons from the relativistic bunch can be analyzed on two scales. On a short timescale, electrons oscillate in the field surrounding the wires, at the frequency c/λ_u, while on a long time scale, the electron beam diverges because the mean field (averaged over λ_u) is defocusing. The electron oscillations and hence the corresponding radiation are characterized by the undulator parameter K and the oscillation wavelength λ_u. As K is approximately proportional to the laser field amplitude, it decreases exponentially with the propagation distance, with a characteristic length $2l_\mathrm{loss}$. The initial value of the undulator parameter K_0 depends on the laser energy and undulator geometry; for the parameters in Table 1, $K_0 \approx 0.7$. In the limit $K \ll 1$ (which is verified after a short propagation), the number of emitted photons per electron oscillation is $\sim 2\alpha K^2$, where $\alpha \simeq 1/137$ is a thin-structure constant [16]. Thus, we estimate that, over their full trajectory, each electron produces $N_{ph} \simeq 2\alpha K_0^2 l_\mathrm{loss}/\lambda_\mathrm{u}$ photons around an energy $\varepsilon_\mathrm{s}[\mathrm{eV}] \simeq 9.5(\varepsilon_\mathrm{e}[\mathrm{MeV}])^2/\lambda_\mathrm{u}[\mu\mathrm{m}]/(1 + K_0^2/2)$. It follows that for a beam charge of 50 pC, the radiation consists of 1.8×10^7 photons with energies centered around 12, 48 and 107 keV, for electron energies of 200, 400 and 600 MeV respectively.

C. Numerical modeling

In order to validate the proposed scheme and to predict more precisely the radiation features, the laser-plasma undulator was modeled using particle-in-cell simulations (see Methods). We considered a quasi-monoenergetic electron beam having the properties given in Table 1, which corresponds to state-of-art laser-plasma accelerators [19–21]. Also shown in Table 1 are the laser parameters at the entrance of the undulator. To prevent the supersonic gas-jet from impacting the nano-wires, a distance of 1 mm between the accelerator and the undulator was chosen, and the drift of the electron in this vaccuum space was self-consistently taken into account. The interaction of the laser and electron beams with a 14-line undulator was modeled in the two-dimension plane $(x\,,y)$.

The two characteristic scales of the electron motion are highlighted in Fig. 3. Figure 3a shows the increase of the electron beam divergence due to the mean transverse field, while Fig. 3b reveals the electron oscillations. The undulator parameter K of each individual particles was calculated from their trajectories over a distance $l_{\rm loss}$. The distribution of K is shown in Fig. 3c and it exhibits a peak around $K = 0.6$, with an average undulator parameter $\langle K\rangle = 0.73$. Simulations also confirm the exponential depletion of the laser (see Fig. 3d). The predicted depletion length $l_{\rm loss} = 0.2$ mm is in a very good agreement with the simulation, which confirms that the laser energy losses are mainly due to the diffraction by the wires. Because the undulator parameter is approximately proportional the square root of the laser intensity, the number of emitted photons per period evolves roughly as the laser energy. It follows that the emission becomes negligible after a propagation exceeding $\sim 3\,l_{\rm loss} = 0.6$ mm.

The synchrotron radiation of an individual electron is emitted in the direction of the electron's velocity, and within a cone of angle $\Delta\theta \sim \gamma_{\rm e}^{-1}$. Therefore, the total radiation emitted by the electron bunch has a minimum angular spread of $\gamma_{\rm e}^{-1}$, but may have a larger spread if the divergence of the bunch exceeds $\gamma_{\rm e}^{-1}$. The energy radiated per units of photon energy and solid angle $\mathrm{d}^2\varepsilon/\mathrm{d}\omega\mathrm{d}\Omega$ is calculated from the Liénard-Wiechert fields. Figure 4 shows the maps of this distribution, in the case of 600 MeV electrons, in the $y = 0$ and $z = 0$ planes (see Fig. 1 for the orientation these axes), and the angular distribution summed over the photon energy. The angular sizes of the source are $\Delta\theta_y = 2.3$ mrad and $\Delta\theta_z = 0.95$ mrad. In the $y = 0$ plane, the photon energy is observed to be distributed around $\hbar c/[\,\lambda_{\rm u}(1 + K^2/2 + \theta_z^2\gamma_{\rm e}^2)\,]$, which is typical for planar undulators. The distribution in the $z = 0$ plane is stretched and flattened due to the growth of the electron beam divergence, which is induced by the undulator averaged transverse field. Also shown in Fig. 4 is the on-axis spectral distribution (red curve). In agreement with the model, the 50 pC electron bunch generates $2.4 \cdot 10^7$ photons in a 33% energy-band (full width at half maximum) centered around 100 keV. The total energy of the X-ray beam in this case is 0.18 μJ and its peak brightness is 4.5×10^{23} photons s^{-1} mm^{-2} mrad^{-2} per 0.1%bandwidth.

Both the photon energy and the source power increase as $\gamma_{\rm e}^2$; they can therefore be tuned by varying the electron energy. This is demonstrated in Fig. 5, where the X-ray peak energy is observed to rise from 12 to 106 keV when the electron energy is increased from 200 to 600 MeV. The relative bandwidth of the emitted spectrum remains constant. This shows that quasi-monoenergetic X-rays can be produced in a wide range of wavelengths.

Discussion

In conclusion, we have presented a new approach that drastically reduces the size, and cost of conventional undulators and that takes full advantage of the high flux electron beams produced in laser-plasma accelerators. This laser-plasma undulator consists of an array of periodically assembled nano-wires which are ionized by the laser pulse exiting from a laser-plasma accelerator, creating a periodic electric field structure that efficiently operates as an electrostatic undulator. We have shown that this approach can produce bright, polarized and quasi-monoenergetic femtosecond X-ray beams with adjustable energies in the range 10-100 keV and a peak brightness of the order of 10^{23} ph.s^{-1}mm^{-2}mrad^{-2} per 0.1% bandwidth, using commercially available laser systems. The source properties could be further improved e.g. by reducing the growth of the divergence inside the undulator. Possible improvements include the design of more complex wire patterns, with uneven spacings, variable wire diameters or wire densities. The use of the nano-structured undulator for coherent amplification of X-rays can also lead to the development of an ultracompact X-ray free electron laser. Moreover, nano-structured laser-plasma devices can be also used to manipulate relativistic particle beams in various ways (e.g. wiggling, collimating focusing). We anticipate that this new approach will open the path for many innovations at the interface between nano-engineering and high-intensity lasers.

Methods

The formation of the plasma undulator by the laser and the motion of the trailing electrons is studied with the PIC code CALDER 2D [22]. The nano-wires are modeled in two dimensions as circles with a radius of 200 nm. They consist of initially neutral atoms of silicon with a density of $5 \cdot 10^{22}$ cm^{-3}. Ionization is accounted for by using the model of Yudin-Ivanov [23, 24]. The undulator includes 14 lines of 25 wires (350 wires in total) with transverse spacing 5.5 μm (period 11 μm) and undulator period $\lambda_{\rm u} = 24$ μm. The moving-window technique

is used to study the propagation of the laser and electron beams over a millimeter (the moving simulation box is 46 μm $\times$ 70 μm). The spatial resolution is of 5 nm.

Velocities and positions of the relativistic electrons are recorded at each 0.5 fs. These trajectories are then used to compute the produced radiation. The spectral distribution of emitted light is calculated using the Fourier components of Lienard-Wiechert potentials in the far field:

$$\frac{\mathrm{d}\mathcal{E}}{\mathrm{d}\Omega\,\mathrm{d}\omega} = \frac{e^2}{4\pi^2 c}\left|\int_{-\infty}^{\infty}\mathrm{d}t\,\frac{\mathbf{n}\times(\mathbf{n}-\boldsymbol{\beta})\times\dot{\boldsymbol{\beta}}}{(1-\mathbf{n}\,\boldsymbol{\beta})^2}\,\mathrm{e}^{i\omega(t-\mathbf{n}\mathbf{r}/c)}\right|^2$$

The integral is calculated in a 3D angular-spectral space for each particle. The average incoherent spectrum emitted by one electron is calculated as the average of the spectra emitted by the macro-particles. For the spectrum calculation $1.5 \cdot 10^4$ macro-particles were used.

[1] Albert C. Thompson et al. *X-RAY DATA BOOKLET*, Center for X-ray Optics and Advanced Light Source, second edition (2001)

[2] Donald H Bilderback, Pascal Elleaume, and Edgar Weckert, Review of third and next generation synchrotron light sources, *J. Phys. B: At., Mol. Opt. Phys.*, 38(9), S773 (2005)

[3] P. Emma et al, First lasing and operation of an ångsrtöm-wavelength free-electron laser, *Nat. Phys.*, 4, 641–647 (2010)

[4] C. Joshi, The development of laser- and beam-driven plasma accelerators as an experimental field, *Phys. Plasmas*, 14(5), 055501 (2007)

[5] E. Esarey, C. B. Schroeder, and W. P. Leemans, Physics of laser-driven plasma-based electron accelerators, *Rev. Mod. Phys.*, 81, 1229–1285 (2009)

[6] V. Malka, Laser plasma accelerators, *Phys. Plasmas*, 19(5), 055501 (2012)

[7] S. M. Hooker, Developments in laser-driven plasma accelerators, *Nat. Photon.*, 7, 775–782 (2013)

[8] J. Faure, C. Rechatin, A. Norlin, A. Lifschitz, Y. Glinec, and V. Malka, Controlled injection and acceleration of electrons in plasma wakefields by colliding laser pulses, *Nature*, 444, 737–739 (2006)

[9] C Thaury, et al, Plasma mirrors for ultrahigh-intensity optics, *Nat. Phys.*, 3(6), 424–429 (2007)

[10] J. Faure et al, Observation of laser-pulse shortening in nonlinear plasma waves, *Phys. Rev. Lett.*, 95, 205003 (2005)

[11] R. Kodama et al, Plasma devices to guide and collimate a high density of MeV electrons, *Nature*, 432(6), 1005–1008 (2004)

[12] Hyung Taek Kim et al, Enhancement of electron energy to the multi-gev regime by a dual-stage laser-wakefield accelerator pumped by petawatt laser pulses, *Phys. Rev. Lett.*, 111, 165002 (2013)

[13] Kazuhisa Nakajima, Compact X-ray sources-Towards a table-top free electron laser, *Nat. Phys.*, 4, 92–93 (2008)

[14] H.-P. Schlenvoigt et al, A compact synchrotron radiation source driven by a laser-plasma wakefield accelerator, *Nat. Phys.*, 4, 130–133 (2008)

[15] Matthias Fuchs et al, Laser-driven soft-x-ray undulator source, *Nat. Phys.*, 5, 826–829, (2009)

[16] Jackson J. D., *Classical Electrodynamics*, John Wiley & Sons, 3nd edition (1998)

[17] V.L. Ginzburg, *The propagation of electromagnetic waves in plasmas*, International series of monographs on electromagnetic waves, Pergamon Press (1970)

[18] F. Brunel, Not-so-resonant, resonant absorption, *Phys. Rev. Lett.*, 59, 52–55 (1987)

[19] R. Weingartner et al, Ultralow emittance electron beams from a laser-wakefield accelerator, *Phys. Rev. ST Accel. Beams*, 15, 111302 (2012)

[20] C. Rechatin et al, Controlling the phase-space volume of injected electrons in a laser-plasma accelerator, *Phys. Rev. Lett.*, 102, 164801 (2009)

[21] A. J. Gonsalves et al, Tunable laser plasma accelerator based on longitudinal density tailoring, *Nat. Phys.*, 7(11), 862–866 (2011)

[22] E. Lefebvre et al, Electron and photon production from relativistic laser–plasma interactions, *Nucl. Fusion*, 43(7), 629 (2003)

[23] Gennady L. Yudin and Misha Yu. Ivanov, Nonadiabatic tunnel ionization: Looking inside a laser cycle, *Phys. Rev. A*, 64, 013409 (2001)

[24] R. Nuter, L. Gremillet, E. Lefebvre, A. Levy, T. Ceccotti, and P. Martin, Field ionization model implemented in particle in cell code and applied to laser-accelerated carbon ions, *Phys. Plasmas*, 18(3), 033107 (2011)

I. ACKNOWLEDGEMENTS

This work was partially supported by the European Research Council through the PARIS ERC project (Contract No. 226424) and X-Five ERC project (Contract No. 339128). The authors acknowledge L. Grémillet and R. Nuter from CEA for providing us with an advanced version of the CALDER code.

II. AUTHOR CONTRIBUTIONS

I.A.A. developed the theoretical description; I.A.A., R.L. and A.L. adapted the code; I.A.A. and R.L. carried out the simulations and with C.T. wrote the paper; A.L. and V.M. proposed the idea of the scheme and supervised the work; K.K. and J.M.R. contributed to the overall project.

III. COMPETING FINANCIAL INTERESTS

The authors have no competing interests as defined by Nature Publishing Group, or other interests that might be perceived to influence the results and/or discussion reported in this article.

Table 1: Design parameters of the source.

Laser system	
Type	Ti:saphirre
Wavelength	0.8 μm
Pulse duration*	30 fs
Pulse energy	0.7 J
Beam radius* σ_{las} (when entering the undulator)	13 μm
Wires configuration	
Material	Si
Diameter	0.4 μm
Undulator period	24 μm
Transverse spacing	5.5μm
LPA electron beam	
Duration*	3.3 fs
Normalized emittance* ϵ_{N}	0.2 mm·mrad
Initial radius* σ_{e} (at the exit of the accelerator)	1 μm
Energy spread*	1 %
Charge	50 pC
Average energy ε_{e}	200 / 400 / 600 MeV
Undulator emission	
Photon energy	12 / 47 / 106 keV
Peak brightness**	0.5 / 2 / 4.5
Bandwidth (FWHM)	33%
Angular sizes*	0.95 mrad$\times$ 2.3 mrad

* RMS values

** in units of 10^{23} photons s^{-1} mm^{-2} mrad^{-2} per 0.1%bandwidth

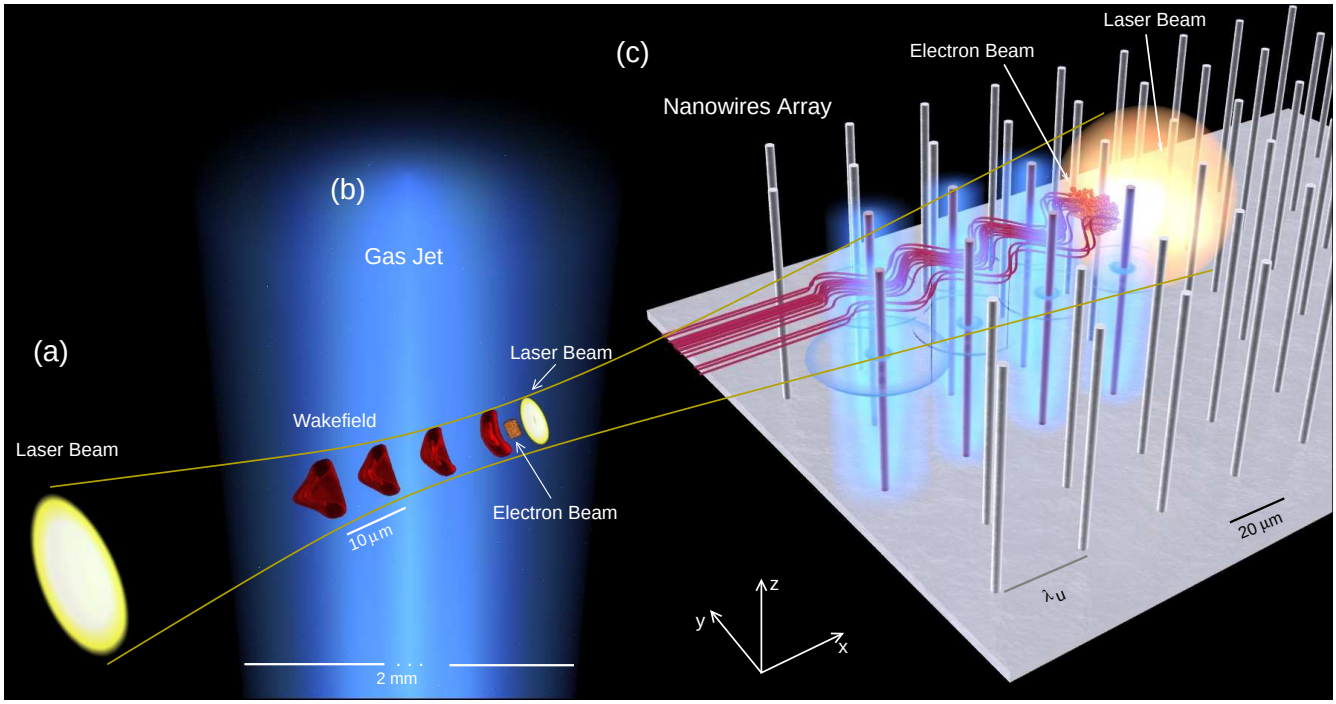

FIG. 1: Principle scheme of a laser-plasma synchrotron. (a) An intense laser pulse (yellow) is focused in a gas jet. (b) The laser pulse propagates through the gas jet, trapping and accelerating an electron bunch in its wake. (c) The laser pulse ionizes the nano-wires, heats their electrons and creates an electrostatic field (in blue). The trailing electron bunch wiggles in this field (red trajectories).

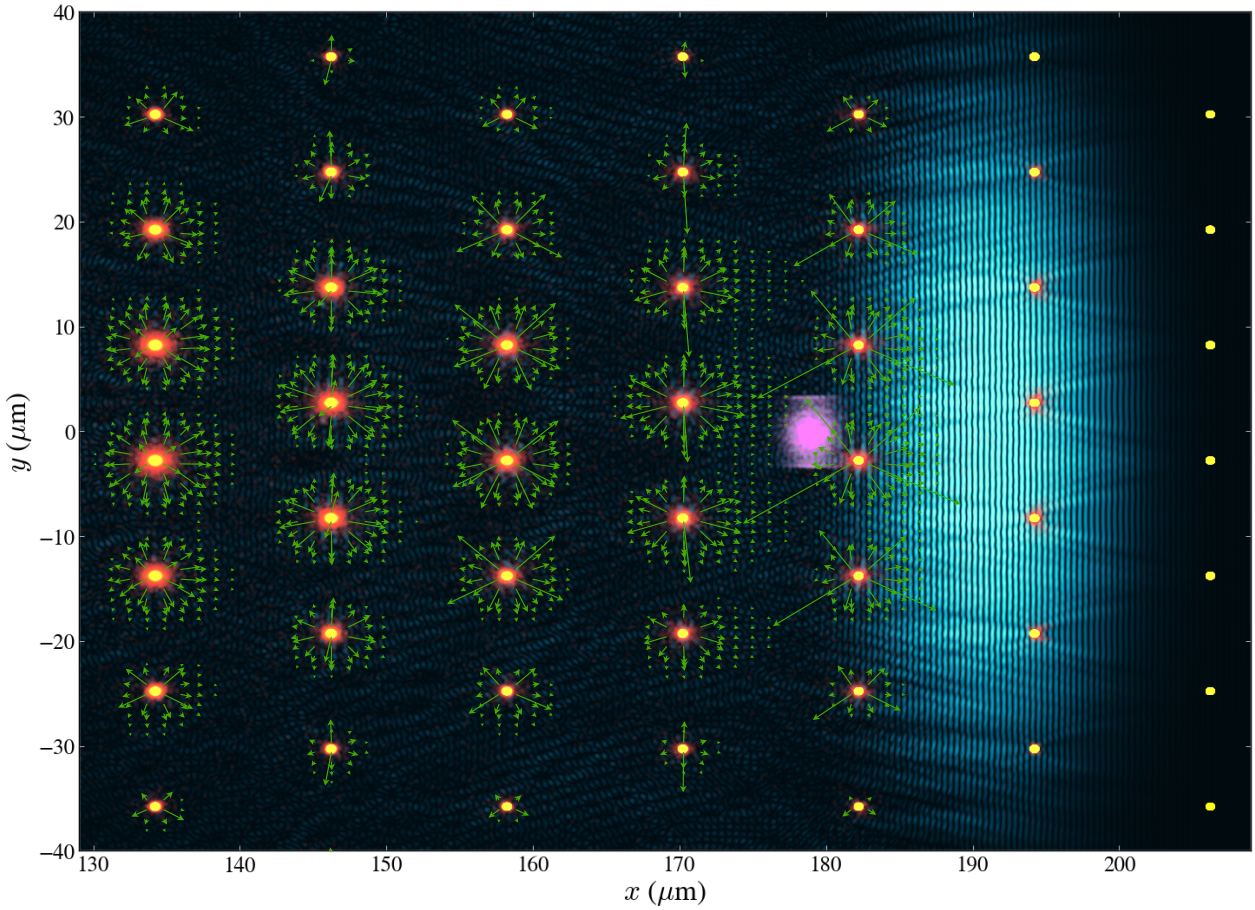

FIG. 2: Snapshot of a particle-in-cell simulation of the laser-plasma undulator. The laser, that propagates from left to right, and the scattered electromagnetic waves are shown in blue tones. The relativistic electron beam, that follows the laser is represented in pink, the ions and the electrons of the wires are shown in yellow and orange respectively. The green vectors represent the electric field generated by the plasma wires. In this simulation the parameters from Table 1 are used.

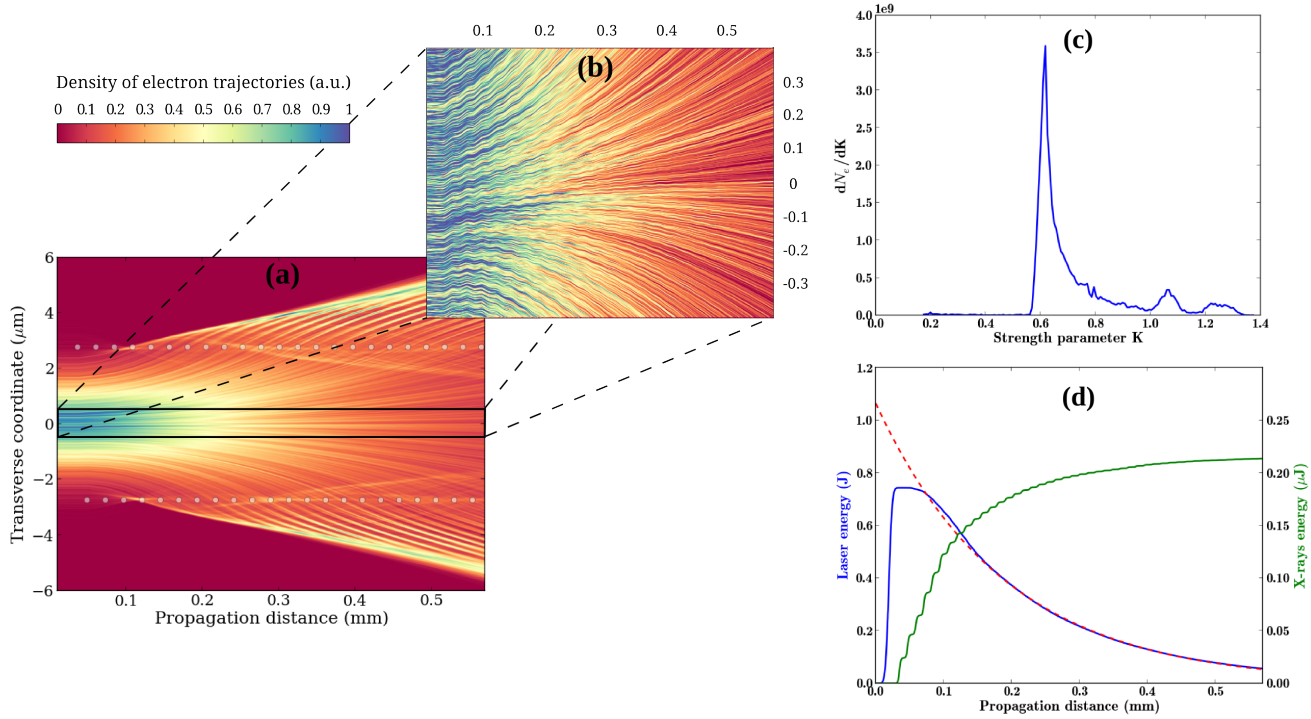

FIG. 3: Electrons and laser propagation in a laser-plasma undulator. (a) Electron trajectories in the undulator, obtained from a 2D PIC simulation. The color scale indicates the electron density, propagation and transverse distances are measured in millimeters and micrometers respectively, and the white markers indicate the positions of the wires. (b) Zoom on the central part of (a). (c) Distribution of the undulator parameter K, calculated from individual trajectories. (d) Evolution of the total emitted energy (green curve), and the total laser energy in the PIC simulation (blue curve) compared with our model $I_{\rm las}(x) \propto \exp(-x/l_{\rm loss})$ with $l_{\rm loss} = 0.2$ mm (red dashed line);

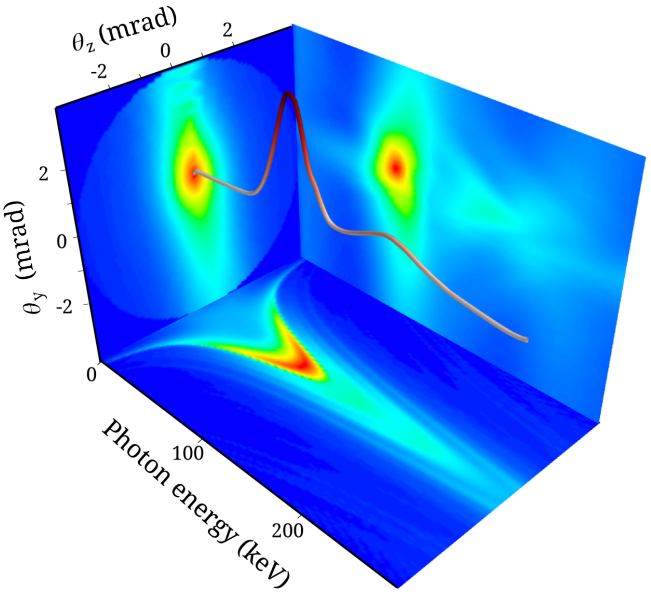

FIG. 4: Angular-spectral distribution of produced X-rays. Maps of the emission energy distributions $\mathrm{d}^2\varepsilon/\mathrm{d}\omega\mathrm{d}\Omega$ in the planes $y = 0$ (horizontal plane) and $z = 0$ (right vertical plane), and energy integrated angular distribution (left vertical plane). The angle θ_y is angular distance along the y axis, while θ_z is that along the z axis. The curve represents the on-axis spectral distribution. The calculation was performed for 600 MeV electrons.

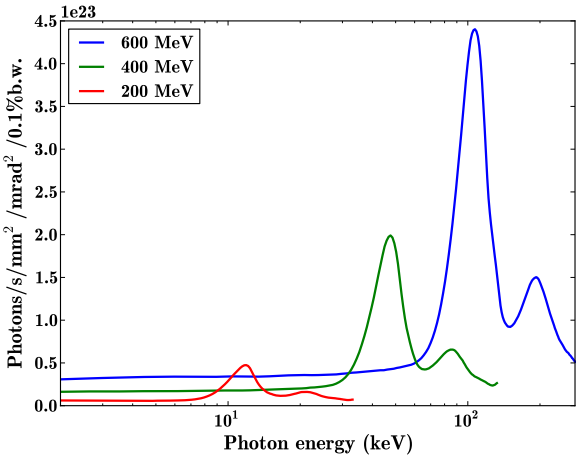

FIG. 5: On-axis X-ray spectra calculated for different electron energies. Spectral distribution of the source brightness is calculated along the propagation direction for electron average energies of 200 MeV (red curve), 400 MeV (green curve) and 600 MeV (blue curve).